P H Y S I C A L   R E V I E W   L E T T E R S

Single-File Charge Storage in Conducting Nanopores

Alpha A. Lee,[1,2] Svyatoslav Kondrat,[2,3] and Alexei A. Kornyshev[2,*]

[1]*Mathematical Institute, University of Oxford, Oxford OX2 6HD, United Kingdom*
[2]*Department of Chemistry, Faculty of Natural Sciences, Imperial College London, London SW7 2AZ, United Kingdom*
[3]*IBG-1: Biothechology, Forschungszentrum Jülich, 52425 Jülich, Germany*
(Received 19 September 2013; revised manuscript received 12 March 2014; published 25 July 2014)

Charging of a conducting tubular nanopore in a nanostructured electrode is treated using an exactly solvable 1D lattice model, including ion correlations screened by ion-image interactions. Analytical expressions are obtained for the accumulated charge and capacitance as a function of voltage. They show that the mechanism of charge storage, and the qualitative form of the capacitance-voltage curve, are sensitive to how favorable it is for ions to occupy the unpolarized pore, and the pore radius. Qualitative predictions of the theory are corroborated by Monte Carlo simulations. These results highlight the effect of ion affinity to unpolarized pores on the charge and energy storage in supercapacitors. Furthermore, they suggest that the question of the occupancy of unpolarized pores could be answered by measuring the capacitance-voltage dependence.

Efficient energy storage is important for the development of new technologies [1,2]. Electrical double-layer super-capacitors (EDLS) which store energy at the electrode-electrolyte interface continue to draw attention because of their high power density and stability [3–7]. Porous electrodes with large surface area are used to maximize energy storage [8]. A marked increase in the capacitance per unit surface area was experimentally observed when the pore size approached the size of an ion [9–11], suggesting a different mechanism of capacitance when ions are confined.

Previous theoretical approaches focused on the role of image charge [12,13] and pore curvature [14–16] in determining the effect of pore size on capacitance. Decreasing the pore size increases the ion-image attraction and screens like-charge repulsion, increasing the capacitance. Simulations using polarizable electrode models corroborated the importance of ion-image interactions [17–22].

The physics of charge storage is more complex, and received considerable attention [12,13,21,23–26]. Simulations reveal that co-ions are expelled from the pore at low voltage, while counterion insertion dominates at high voltages [21,27,28]. However, the extent of ion occupation in an unpolarized pore is the topic of debate; some simulations suggest the pores are occupied [21,22,27], while others suggest the contrary [23–25]. In addition, the amount of ions in the pore at peak capacitance is as yet inconclusive. Answers to those questions are required for the optimization of nanoporous supercapacitors.

To elucidate the mechanism of charge storage in a tubular nanopore, we consider a 1D lattice of lattice constant $2a$, with a the ion radius (see Fig. 1). The lattice sites are occupied by either cations ($S = 1$), anions ($S = -1$), or voids or an uncharged solvent ($S = 0$). The choice of 1D lattice is justified when the cations and anions are of comparable size, and are lined up in single file. This is expected to hold for narrow pores ($R \sim a$), where the capacitance (per unit surface area) is maximal. In this configuration, each ion experiences the same electrostatic potential. Furthermore, we assume that ions interact with their nearest neighbors only. Although the Coulomb potential in free space is long-ranged, electrostatic interactions are strongly screened in metallic pores and decay exponentially. The interaction energy of two monovalent point charges located at the center of a metallic cylinder of radius R separated by distance z is given by [29]

$$\frac{V(z)}{k_B T} = 2 \frac{L_B^{\text{pore}}}{R} \sum_{m=1}^{\infty} \frac{\exp(-\frac{k_m z}{R})}{k_m [J_1(k_m)]^2}, \qquad (1)$$

where $L_B^{\text{pore}} = e^2/(\varepsilon_\infty k_B T)$ is the Bjerrum length in the pore with dielectric constant ε_∞, and k_m are zeros of $J_0(x)$. Constrained ionic motion within the pore meant that effectively only electronic degrees of freedom contribute to dielectric screening and we assume $\varepsilon_\infty = 2$ [30]. Experimentally sub-nanometer tubular nanopores comprised of noble metals and alloys have been reported [31–34]. For semimetallic pores with thick walls, electrostatic interactions within the Thomas-Fermi model are still exponential albeit with a renormalized pore radius accounting for electric field penetration into the material [13,35,36]. For simplicity, we focus here on metallic cylindrical nanopores, although our model only assumes narrow tubular pores and screened electrostatic interactions.

The Hamiltonian of the system is

$$\frac{\mathcal{H}}{k_B T} = J \sum_i S_i S_{i+1} + \frac{1}{2} \sum_i (\mu_{S_i} S_i + \mu_{S_{i+1}} S_{i+1}), \qquad (2)$$

where $J = V(2a)/k_B T$ is the effective ion-ion interaction energy, and

$$\mu_{S=\pm 1} = u \mp w_\pm, \qquad \mu_{S=0} = 0, \qquad (3)$$

048701-1
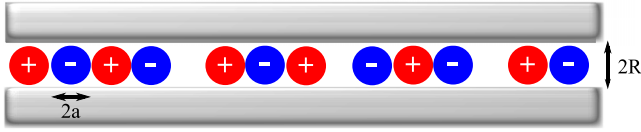
FIG. 1 (color online).   1D lattice model for charge storage in a cylindrical nanopore. R is the pore radius and $2a$ is the lattice constant.

where $u = e\psi/k_BT$ is the dimensionless electrostatic potential of the pore, and $w_\pm$ is the energy of transfer of *one* cation or anion from the pore to the bulk in units of k_BT. In general, $w_+ \neq w_-$ due to the specific chemical interactions between the ion and the pore surface, and will be treated as model parameters, characterizing the propensity for ions to occupy the pore at zero voltage (see [38]). It has been shown [44] that for Hamiltonians with nonlocal interactions, a mean-field theory can be more adequate than resorting to nearest neighbor interactions. In our case, however, the strong exponential screening of ion-ion interactions makes the nearest-neighbor treatment appropriate, as is indirectly confirmed by a good qualitative agreement with more robust Monte Carlo simulations (see below).

Hamiltonian (2) is analogous to the Blume-Emery-Griffiths (BEG) model describing magnetism with spin-1 nuclei [45], except introducing an effective chemical potential that couples the ions to the bulk [46]. The exact partition function can be obtained by evaluating the trace of the transfer matrix T of Hamiltonian (2),

$$T = \begin{pmatrix} e^{-J-\mu_+} & e^{-(\mu_+/2)} & e^{J-(1/2)(\mu_+-\mu_-)} \\ e^{-(\mu_+/2)} & 1 & e^{(\mu_-/2)} \\ e^{J-(1/2)(\mu_+-\mu_-)} & e^{(\mu_-/2)} & e^{-J+\mu_-} \end{pmatrix}. \quad (4)$$

In the thermodynamic limit the number of lattice sites $N \to \infty$, and only the largest eigenvalue of the transfer matrix contributes to thermodynamic properties. The largest eigenvalue of T is given by [49,50]

$$\lambda = \frac{1}{3}[1 + 2e^{\bar{w}-J}\cosh(u-\delta w)] + \frac{2\Lambda^{1/2}}{3}\cos\left[\frac{1}{3}\cos^{-1}\frac{\Delta}{2\Lambda^{3/2}}\right], \quad (5)$$

where Λ and Δ depend on $u - \delta w$, J and $\bar{w}$, and $\delta w = (w_+ - w_-)/2$ and $\bar{w} = (w_+ + w_-)/2$ [51].

The total ionic charge per unit surface area is given by

$$\sigma = \frac{e}{2ap}\langle S_i \rangle = \frac{e}{2apN}\frac{d\mathcal{F}}{du}, \quad (6)$$

where $\mathcal{F} = -\ln Z$ is the Helmholtz free energy in units of k_BT, $Z = \lambda^N$ is the partition function, and p is the circumference of the pore. Thus,

$$\sigma = \frac{e}{2ap}\frac{1}{\lambda}\left\{\frac{2}{3}e^{\bar{w}-J}\sinh(u - \delta w)\right.$$
$$+ \frac{\Lambda_u}{3\sqrt{\Lambda}}\cos\left[\frac{1}{3}\cos^{-1}\frac{\Delta}{2\Lambda^{3/2}}\right] + \frac{1}{9}\left(2\Delta_u - 3\frac{\Delta\Lambda_u}{\Lambda}\right)$$
$$\left. \times \sqrt{\frac{\Lambda}{4\Lambda^3 - \Delta^2}}\sin\left[\frac{1}{3}\cos^{-1}\left(\frac{1}{2}\frac{\Delta}{\Lambda^{3/2}}\right)\right]\right\}, \quad (7)$$

where $\Lambda_u = \partial\Lambda/\partial u$ and $\Delta_u = \partial\Delta/\partial u$.

Consider an example: cations and anions with $w_+ = w_- = w$ [52], ion radius $a = 5$ Å, pore radius $R = 5.02$ Å and by Eq. (1) $J = 1.6$. Figure 2(a) shows that at low voltages the anion population is almost constant while cations are removed from the pore, decreasing the total ion

(a)

(b)
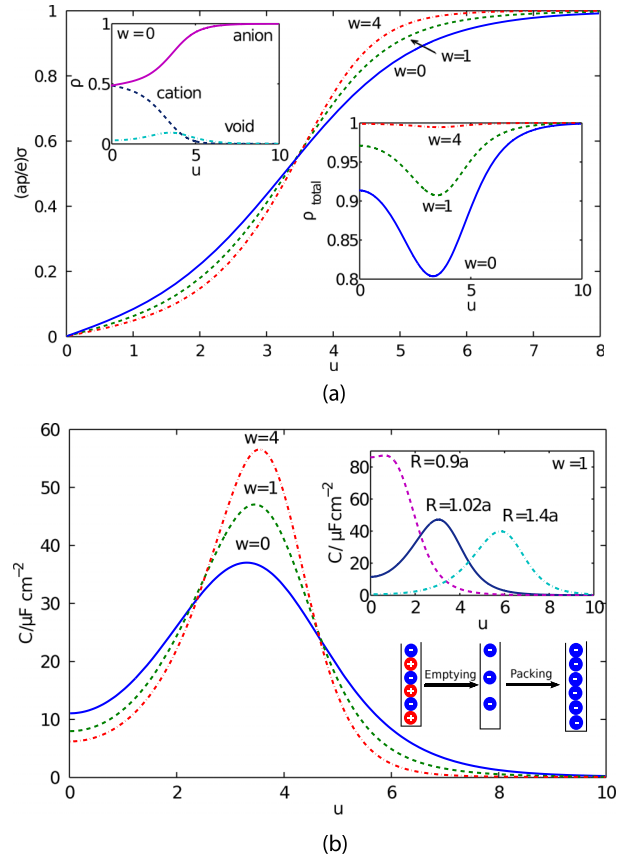
FIG. 2 (color online).   Ionophilic pores: charge storage occurs via removing co-ions at low voltages and filling the pore with counterions at large voltages. (a) The main panel shows the dimensionless surface charge density $(2ap/e)\sigma$ with increasing voltage, plotted for various values of transfer energy w. The insets show the number density of cations and anions $\rho_\pm = (1/Z)(\partial Z/\partial\mu_\pm)$, when $w = 0$ and the total density of ions $\rho_{total} = \rho_+ + \rho_-$ with increasing voltage, both normalized with respect to the maximum density. (b) Maximum differential capacitance increases as the transfer energy increases and the pore size decreases. The differential capacitance is symmetric about $u = 0$, and the $R < a$ case corresponds to elongated (e.g., elliptical) ions. All curves are plotted for $J = 1.6$ ($R = 1.02a$), except of the inset in (b).

density. The ion density reaches a minimum as the cations are almost depleted (at $u \approx 4$), and then anions start entering the pore.

An experimentally measurable quantity of EDLS is the differential capacitance, $C = -(e/k_B T)d\sigma/du$. Figure 2(b) shows that the threshold voltage for anions to enter the pore increases and the peak in differential capacitance becomes sharper as w increases (i.e., the pore is more "ionophilic"). Exchanging cations with voids is no longer favorable, and charging is due to swapping cations with anions. This occurs when the unfavorable interaction between cation and applied potential surpasses the cation-anion attraction. Decreasing the pore size enhances the screening of electrostatic interactions and it becomes easier to unbind unlike charges and pack like charges. This shifts the maximum in differential capacitance towards lower voltages. The height of the maximum increases as the pore size (hence, J) decreases [see inset of Fig. 2(b)], in agreement with experimental observation [9].

For strongly ionophilic pores (large positive w), the population of voids is always negligible and Hamiltonian (2) is analogous to the standard two-state Ising model, $S = \pm 1$ [53], affording a simple expression for the differential capacitance [26],

$$C = C_0 \frac{e^{4J}\cosh u}{(\sinh^2 u + e^{4J})^{3/2}}, \qquad (8)$$

where $C_0 = e^2/2k_B Tap$ ($\approx 2.0a/R$ F m^{-2} for room temperature and $a = 5$ Å). At small voltages, $C/C_0 \approx e^{-2J} + (1/2)e^{-6J}(e^{4J} - 3)u^2$. For $J > (1/4)\ln 3$, the maximum differential capacitance is achieved at $u = \ln\sqrt{e^{4J} - 2 + (e^{8J} - 4e^{4J} + 3)^{1/2}} \approx 2J$ (for $J \gg 1$), showing that the swapping of cations with anions commences only when the interaction with the applied potential is larger than like-charge repulsion. When the ion-ion interaction is weak [$J < (1/4)\ln 3$], cation-anion swapping is facile and the maximum is reached at $u = 0$ with $C_{\max} = C_0 e^{-2J}$. This changeover in charging mechanism is in line with the experimental observations [54]. There, a peak in capacitance is observed when the average pore size is large (9.4 Å) and a monotonic decrease is seen for narrower pores (8.7 Å), where the ion diameter ≈ 8 Å [55].

We now consider ionophobic pores ($w < 0$), which may occur when ions have large bulk entropy compared with their entropy in the pore, or when there are repulsive ion-surface chemical interactions. Figure 3 shows that two maxima emerge in the differential capacitance for large negative w. These shift to higher voltages as w becomes more negative. The one-to-two peak transition occurs at a threshold value of w where $\rho_\pm = 1/3$ at zero applied voltage. This is also when the initial decrease in the total ion density, ρ_{total}, disappears and the nonpolarized pore is essentially empty (see insets in Fig. 3).

The two peaks in capacitance arise as ions first need to overcome ion-surface repulsion to enter the pore and,
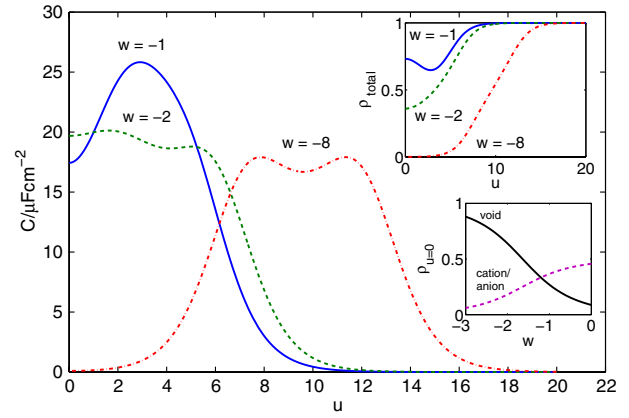
FIG. 3 (color online). Ionophobic pores: the main panel shows that the differential capacitance emerges as two peaks when the transfer energy becomes more negative. The insets show how the total density varies with voltage for different transfer energies, and how the population of cation, anion and void vary at zero applied potential with transfer energy. In all curves $J = 1.6$ ($R = 1.02a$).

subsequently, the ion-ion like-charge repulsion after the ions begin to accumulate. In the limit of large negative w, the population of cations in the pore is always negligible and the system reduces to a 2-spin model with $S = -1, 0$ for positive applied potentials (see Supplemental Material [38]). The capacitance in this limit is given by

$$C = C_0 \frac{2e^J \cosh[\frac{1}{2}(J - u - w)]}{[2\cosh(J - u - w) + 4e^J - 2]^{3/2}}. \qquad (9)$$

When $J > \ln 3$, there are two maxima at $u = -\ln\left[e^w -2e^{w-J} + \sqrt{e^{2(w-J)}(e^J - 3)(e^J - 1)}\right] \approx -w$ and $u = -\ln\left[e^w - 2e^{w-J} - \sqrt{e^{2(w-J)}(e^J - 3)(e^J - 1)}\right] \approx 2J - w$ (for $J \gg 1$), and minimum at $u = J - w$. Thus, the first stage of the charging process consists of counterions trying to enter the pore, which is only possible when the interaction energy with applied potential overcomes the unfavorable transfer energy ($u \approx -w$). The second stage commences when ions overcome like-charge repulsion and pack closer, which occurs when the interaction energy with applied potential equals the ion-ion repulsion energy ($u \approx 2J - w$, see also [57]). For smaller J, ion-ion repulsion is less unfavorable, and the two stages merge together, resulting in a single peak at $u = J - w$ (cf. Fig. 5). Interestingly, the two peaks can be interpreted as resulting from particle-hole symmetry [57]. One peak in the differential capacitance is seen when $w > 0$ as the system only needs to overcome ion-ion repulsion.

The second peak in the differential capacitance may be exaggerated by the lattice model as, in fact, like charges can position themselves closer to each other continuously. Grand canonical Monte Carlo simulations (see Fig. 4 and Supplemental Material [38] for details) corroborate
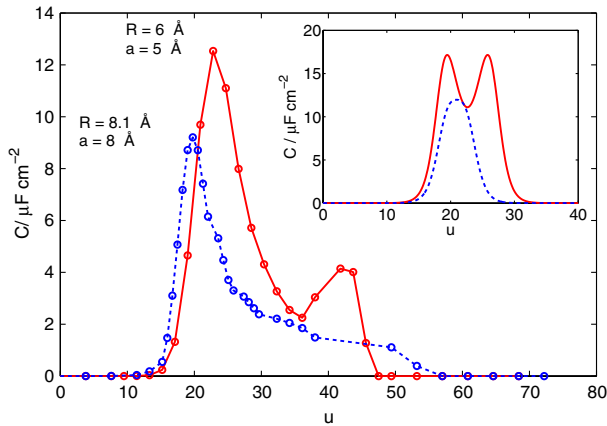
FIG. 4 (color online).   Ionophobic pores: the main panel shows the differential capacitance obtained via Monte Carlo simulation for $(R, a) = (5, 6)$ Å $(J = 2.6)$, and $(R, a) = (8, 8.1)$ Å $(J = 0.92)$. The inset shows the capacitance predicted by the theory. The curves are plotted for $w = -20$.

qualitatively the one-to-two peak transition when the ion-ion interaction decreases. Heuristically, the screening length of the electrostatic interactions acts as a natural length scale even in the off-lattice case. The peaks in differential capacitance predicted by the theory and simulation agree closely. The difference in the magnitude and position of the second peak reflects that lateral entropy and off-lattice effects (e.g., breaking particle-hole symmetry; see [57]) make the second charging process less abrupt and occurring over a broader range of voltages.

The utility of supercapacitors lies in efficient charge storage. The stored energy density is given by $\mathfrak{E}(u) = \int_0^u VC(V)dV$. The inset of Fig. 5 shows that at low voltages, ionophilic capacitors ($w > 0$) readily charge
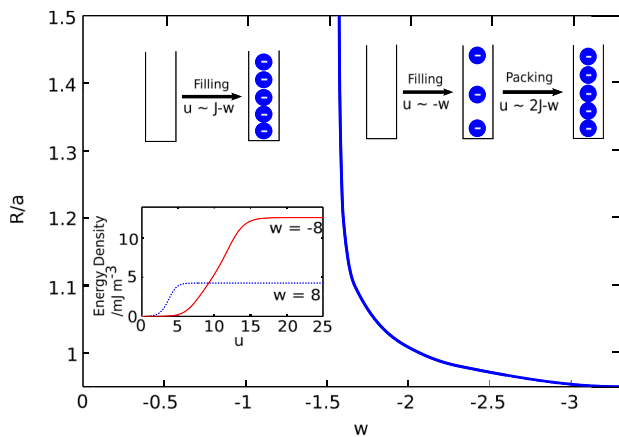
FIG. 5 (color online).   A main panel shows a map of different charging regimes with negative transfer energy. With $w \ll 0$, ions need to first overcome the energy penalty associated with entering the pore ("filling"), and, subsequently, packing themselves close together. For less negative values w, the two charging processes merge together. The inset shows how the stored energy density varies with applied voltage for different values of w. The figures are plotted with $a = 5$ Å.

and store a larger amount of energy. For strongly ionophobic pores, charges only enter the pores after $u \approx -w$, but the system does more work to draw the charges in. Therefore, for high voltages, ionophobic capacitors achieve larger energy density. Thus, the model predicts that systems with favorable ion-surface interaction are optimal for low voltage applications, whereas those with unfavorable interactions are optimal for high voltage applications. Such interactions can be manipulated by altering the chemical composition of the ion and the pore.

Conclusion.—We considered the charging of a tubular nanopore in a 1D lattice model, and showed that the mechanism of charge storage depends on the pore size and interaction between ions and the nanopore surface. Three distinct charging mechanisms were identified. With small pore size, the system first expels the co-ions before filling the pore with counterions. When the energy penalty for ions to enter the pore is large, pore filling only commences when the interaction energy with applied potential is larger than the ion-pore repulsive interaction. A separate stage of "ion packing" starts after interaction with the applied potential surpasses ion-ion repulsion. This agrees qualitatively with Monte Carlo simulations. Experimental data on the capacitance-voltage dependence in nanostructured electrodes are currently scarce, and our model suggests a possible experimental handle to study the different regimes of charge storage [60].

Our theory is based on thermodynamics—kinetic considerations suggest that ionophobic pores charge faster. Ionophilic pores, despite being able to store more energy at low applied voltage (cf. Fig 5), can only charge by "swapping" out co-ions, which is slow for longer pores. This process could be accelerated if the pore wall or the ions are deformable, or ion shape anisotropy allows ions to slide past each other. Those finer kinetic aspects are considered elsewhere [61].

*a.kornyshev@imperial.ac.uk

[1] J. Miller and P. Simon, Science **321**, 651 (2008).
[2] M. Lu, F. Beguin, and E. Frackowiak, *Supercapacitors: Materials, Systems and Applications* (John Wiley & Sons, New York, 2013).
[3] B. Conway, *Electrochemical Supercapacitors: Scientific Fundamentals and Technological Applications* (Springer, New York, 1999).
[4] P. Simon and Y. Gogotsi, Nat. Mater. **7**, 845 (2008).
[5] P. Simon and Y. Gogotsi, Acc. Chem. Res. **46**, 1094 (2013).
[6] A. Burke, J. Power Sources **91**, 37 (2000).

[7] A. Burke, Proc. IEEE **95**, 806 (2007).

[8] P. Simon and Y. Gogotsi, Phil. Trans. R. Soc. A **368**, 3457 (2010).

[9] J. Chmiola, G. Yushin, Y. Gogotsi, C. Portet, P. Simon, and P. Taberna, Science **313**, 1760 (2006).

[10] C. Largeot, C. Portet, J. Chmiola, P. Taberna, Y. Gogotsi, and P. Simon, J. Am. Chem. Soc. **130**, 2730 (2008).

[11] R. Lin, P. Huang, J. Segalini, C. Largeot, P.-L. Taberna, J. Chmiola, Y. Gogotsi, and P. Simon, Electrochim. Acta **54**, 7025 (2009).

[12] S. Kondrat and A. Kornyshev, J. Phys. Condens. Matter **23**, 022201 (2011).

[13] B. Skinner, T. Chen, M. S. Loth, and B. I. Shklovskii, Phys. Rev. E **83**, 056102 (2011).

[14] J. Huang, B. Sumpter, and V. Meunier, Angew. Chem., Int. Ed. **47**, 520 (2008).

[15] J. Vatamanu, O. Borodin, and G. Smith, Phys. Chem. Chem. Phys., **12**, 170 (2010).

[16] J. Huang, B. Sumpter, and V. Meunier, Chem. Eur. J. **14**, 6614 (2008).

[17] G. Feng, R. Qiao, J. Huang, B. Sumpter, and V. Meunier, J. Phys. Chem. C **114**, 18 012 (2010).

[18] G. Feng, R. Qiao, J. Huang, B. Sumpter, and V. Meunier, ACS Nano **4**, 2382 (2010).

[19] M. S. Loth, B. Skinner, and B. I. Shklovskii, Phys. Rev. E **82**, 056102 (2010).

[20] P. Wu, J. Huang, V. Meunier, B. Sumpter, and R. Qiao, ACS Nano **5**, 9044 (2011).

[21] S. Kondrat, N. Georgi, M. Fedorov, and A. Kornyshev, Phys. Chem. Chem. Phys. **13**, 11 359 (2011).

[22] C. Merlet, B. Rotenberg, P. Madden, P. Taberna, P. Simon, Y. Gogotsi, and M. Salanne, Nat. Mater. **11**, 306 (2012).

[23] K. Kiyohara, T. Sugino, and K. Asaka, J. Chem. Phys. **132**, 144705 (2010).

[24] K. Kiyohara, T. Sugino, and K. Asaka, J. Chem. Phys. **134**, 154710 (2011).

[25] K. Kiyohara, H. Shioyama, T. Sugino, and K. Asaka, J. Chem. Phys. **136**, 094701 (2012).

[26] A. A. Kornyshev, Faraday Discuss. **164**, 117 (2013).

[27] P. Wu, J. Huang, V. Meunier, B. Sumpter, and R. Qiao, J. Phys. Chem. Lett. **3**, 1732 (2012).

[28] L. Xing, J. Vatamanu, O. Borodin, and D. Bedrov, J. Phys. Chem. Lett. **4**, 132 (2013).

[29] E. Weber, J. Appl. Phys. **10**, 663 (1939).

[30] Generally, the value of ε_∞ can vary depending on the amount of voids or neutral solvent in the pore, and the pore width. However, this is not expected in neat ionic liquid.

[31] M. Kim, G. H. Jeong, K. Y. Lee, K. Kwon, and S. W. Han, J. Mater. Chem. **18**, 2208 (2008).

[32] C. C. Buttner, A. Langner, M. Geuss, F. Muller, P. Werner, and U. Gosele, ACS Nano **3**, 3122 (2009).

[33] F. Bian, Y. Tian, R. Wang, H. Yang, H. Xu, S. Meng, and J. Zhao, Nano Lett. **11**, 3251 (2011).

[34] T. F. Esterle, D. Sun, M. R. Roberts, P. N. Bartlett, and J. R. Owen, Phys. Chem. Chem. Phys. **14**, 3872 (2012).

[35] C. C. Rochester, A. A. Lee, G. Pruessner, and A. A. Kornyshev, ChemPhysChem **14**, 4121 (2013).

[36] For pores with thin walls such as graphene sheets, the situation may be different [37].

[37] B. Skinner, M. M. Fogler, and B. I. Shklovskii, Phys. Rev. B **84**, 235133 (2011).

[38] See Supplemental Material at http://link.aps.org/supplemental/10.1103/PhysRevLett.113.048701, which includes Refs. [39–43]

[39] C. Bouwkamp and N. De Bruijn, J. Appl. Phys. **18**, 562 (1947).

[40] P. Holoborodko, http://www.holoborodko.com/pavel/numerical-methods/numerical-derivative/smooth-low-noise-differentiators/.

[41] M. G. Martin, http://towhee.sourceforge.net/.

[42] R. Lynden-Bell, J. Chem. Phys. **129**, 204503 (2008).

[43] D. Roy and M. Maroncelli, J. Phys. Chem. B **116**, 5951 (2012).

[44] Y. Burak and R. R. Netz, J. Phys. Chem. B **108**, 4840 (2004).

[45] M. Blume, V. Emery, and R. Griffiths, Phys. Rev. A **4**, 1071 (1971).

[46] The classical BEG model has been solved perturbatively in the limit of low applied field [47,48]. However, we obtain the exact solution in this work.

[47] T. Obokata and T. Ooucrn, J. Phys. Soc. Jpn. **25**, 322 (1968).

[48] M. Suzuki, B. Tsujiyama, and S. Katsura, J. Math. Phys. (N.Y.) **8**, 124 (1967).

[49] D. Zwillinger, *CRC Standard Mathematical Tables and Formulae* (CRC Press, Boca Raton, 2011).

[50] J. Kopp, Int. J. Mod. Phys. C **19**, 523 (2008); **19** 845(E) (2008).

[51] $\Lambda = 2e^{\bar{w}-J}\cosh(u-\delta w)(2e^{\bar{w}-J}\cosh(u-\delta w)+3e^J-1)+ 6e^{2\bar{w}}\sinh 2J+1$ and $\Delta = -6e^{2\bar{w}}[5(\sinh 2J-3\sinh J)+ \cosh 2J-3\cosh J]+2e^{\bar{w}-J}(3e^J-1)\{3e^{\bar{w}-J}\cosh[2(u-\delta w)]+ \cosh(u-\delta w)\}+2e^{3(\bar{w}-J)}\cosh(u-\delta w)(4\cosh[2(u-\delta w)]+ 9e^{4J}-5)+2$.

[52] For $w_+ \neq w_-$, the capacitance-voltage curves will only shift.

[53] D. Chandler, *Introduction to Modern Statistical Mechanics* (Oxford University Press, New York, 1987).

[54] S. Kondrat, C. Perez, V. Presser, Y. Gogotsi, and A. Kornyshev, Energy Environ. Sci. **5**, 6474 (2012).

[55] In Ref. [54], the porous electrodes were fabricated by chlorination of carbides with wide or narrow pores corresponding to high or low chlorination temperatures. Some experiments [56] indicate that at low chlorination temperatures, there is an abundance of cylindrical and spherical pores. Thus, the presence of cylindrical pores, in combination with the results of Fig. 2(b), may explain the peak to no-peak transition observed in Ref. [54].

[56] J. Palmer, A. Llobet, S.-H. Yeon, J. Fischer, Y. Shi, Y. Gogotsi, and K. Gubbins, Carbon **48**, 1116 (2010).

[57] The microscopic lattice Hamiltonian for strongly ionophobic pores [$S = (0, -1)$, see Supplemental Material [38]] exactly fulfills particle-hole symmetry $S_i \rightarrow -S_i - 1$ with shifted energy and voltage ($u \rightarrow 2J - u - w$), in analogy with [58,59].

[58] A. L. Efros, Phys. Rev. B **45**, 11 354 (1992).

[59] B. Skinner and B. I. Shklovskii, Phys. Rev. B **87**, 035409 (2013).

[60] Our model assumes monodisperse pores which are experimentally realizable [34]. Weak polydispersity will reduce and broaden the peaks in capacitance [54], but the qualitative features shall remain intact.

[61] A. A. Lee, S. Kondrat, G. Oshanin, and A. A. Kornyshev, Nanotechnology **25**, 315401 (2014).